The impact of global freshwater forcing on the thermohaline circulation: adjustment of North Atlantic convection sites in a CGCM

D. Swingedouw · P. Braconnot · P. Delecluse · E. Guilyardi · O. Marti

Abstract On the time scale of a century, the Atlantic thermohaline circulation (THC) is sensitive to the global surface salinity distribution. The advection of salinity toward the deep convection sites of the North Atlantic is one of the driving mechanisms for the THC. There is both a northward and a southward contributions. The northward salinity advection (Nsa) is related to the evaporation in the subtropics, and contributes to increased salinity in the convection sites. The southward salinity advection (Ssa) is related to the Arctic freshwater forcing and tends on the contrary to diminish salinity in the convection sites. The THC changes results from a delicate balance between these opposing mechanisms. In this study we evaluate these two effects using the IPSL-CM4 ocean-atmosphere-sea-ice coupled model (used for IPCC AR4). Perturbation experiments have been integrated for 100 years under modern insolation and trace gases. River runoff and evaporation minus precipitation are successively set to zero for the ocean during the coupling procedure. This allows the effect of processes Nsa and Ssa to be estimated with their specific time scales. It is shown that the convection sites in the North Atlantic exhibit various sensitivities to these processes. The Labrador Sea exhibits a dominant sensitivity to local forcing and Ssa with a typical time scale of 10 years, whereas the Irminger Sea is mostly sensitive to Nsa with a 15 year time scale. The GIN Seas respond to both effects with a time scale of 10 years for Ssa and 20 years for Nsa. It is concluded that, in the IPSL-CM4, the global freshwater forcing *damps* the THC on centennial time scales.

1 Introduction

The global conveyor belt (Broecker 1991) is responsible for a northward ocean heat transport in the North Atlantic of about 10^{15} W, thus being a major mechanism of heat distribution between the equator and poles. A weakening of the ocean circulation is likely to diminish the Atlantic Ocean heat transport and to have a cooling effect on Europe (Rahmstorf and Ganopolski 1999). The ocean heat transport is closely related to the thermohaline circulation (hereafter THC). Present day climate models predict a wide range of behaviors for the thermohaline circulation in the future (IPCC 2001). Most of them show a THC weakening under global warming conditions, whereas others do not react. This uncertainty on the future of this deep oceanic circulation also implies an uncertainty for the earth's climate.

It is due to the sensitivity of the THC to several processes. Most of them are not well understood and represented in state-of-the-art CGCMs (coupled general circulation model). On a time scale of a century, the North Atlantic branch of the THC seems mostly sensitive to preconditioning by ice and atmosphere fluxes over the Labrador, Irminger and GIN Seas convection sites (Stouffer and Manabe 2003). The winter cooling by

D. Swingedouw (✉) · P. Braconnot · P. Delecluse · E. Guilyardi · O. Marti
IPSL/Laboratoire des Sciences du Climat et de l'Environnement, Orme des merisiers, 91191 Gif-sur-Yvette, France
e-mail: didier.swingedouw@cea.fr

E. Guilyardi
CGAM, University of Reading, Reading, UK

the atmosphere is necessary to produce local instabilities and deep water formation in the North Atlantic, but salinity also plays a crucial role. Density is strongly sensitive to salinity at high latitudes. For example, for a temperature below 10°C, a cooling of 1.1°C is necessary to increase density by 0.1 kg/m^3, against an increase of only 0.012 PSU for salinity. Another important point is that sea surface salinity (SSS) is not damped by surface freshwater fluxes as is the sea surface temperature (SST) by heat fluxes, because of the absence of direct negative feedback between SSS and surface freshwater forcing. SSS has more degrees of freedom to respond to climate change than does the SST field. There is thus a need to quantify how change in freshwater forcing affects this region, considering the relative effects of the local forcing and advection from the ocean circulation.

Three major convection sites have been identified in the North Atlantic. They are respectively located in the Labrador, Irminger and GIN Seas (Fig. 1). They contribute to deep water formation and thereby to the lower branch of the THC. Several competitive processes determine the SSS in the convection sites (see Fig. 1):

1. the local upper ocean freshwater budget;
2. the southward advection of fresh water from the Arctic, leading to a negative salinity tendency,

referred to as southward salinity advection (Ssa) in the remainder of the paper;
3. the northward salinity advection from the tropics (Nsa);
4. the sea-ice interaction.

Those first three processes are the focus of this study since they have been suggested to play a major role in the behavior of the THC response to increase of CO_2 concentration. For example, Dixon et al. (1999) attribute the reduction of the THC in the GFDL model to an increase of meridional moisture transport leading to more precipitation at high latitudes. Processes 1 and 2 are dominant in their simulation. On the other hand, Latif et al. (2000) show with the ECHAM4/OPYC model that the THC was stabilized by process 3. It was attributed to a change in El Nino variability, enhancing zonal moisture transport from the Atlantic to the Pacific basin and increasing salinity in the tropical Atlantic. Mikolajewicz and Voss (2000) find in scenarios with the ECHAM3/LSG model that the THC is weakened mostly because of the atmosphere temperature rising, leading to a decrease of surface density in the convection sites that stabilizes them. Changes in the global salinity field have almost no effect on the THC,
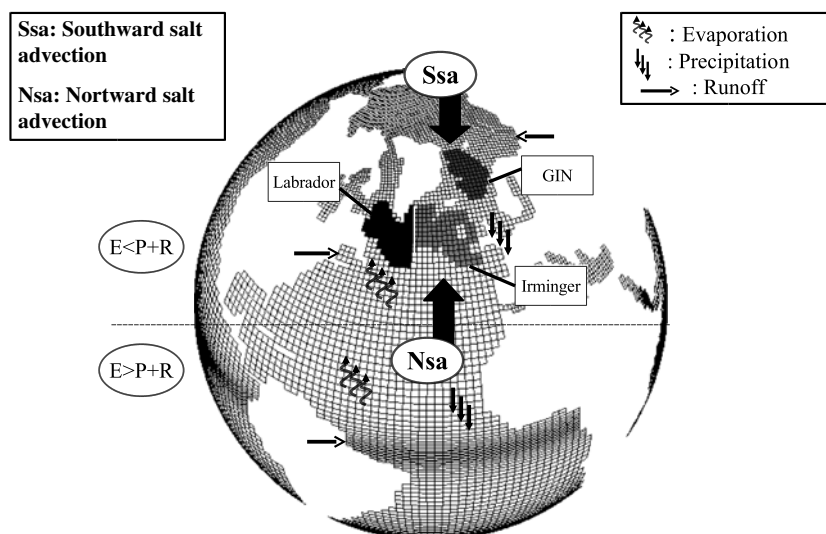
Fig. 1 Schematic view of the Atlantic ocean with the different processes discussed in the study. A focus is made on the convection sites. Different processes are studied: northward salinity transport (*Nsa*), southward salinity transport (*Ssa*) and local freshwater forcing. All of them are related to the global freshwater forcing, evaporation minus precipitation ($E - P$) and runoff (R). The inequality $E < P + R$ and $E > P + R$ are associated to the horizontal dotted line, and represents schematically the region where E dominates $P + R$, in the tropics, and the region where $P + R$ dominates E, north of the *dotted line*. The convection sites appear in *black* for the Labrador Sea (48°N–66°N × 42°W–61°W), in *light gray* for the Irminger Sea (48°N–66°N × 42°W–10°W) and in heavy gray for the GIN Seas (66°N–80°N × 14°W–20°E). These sites do not correspond to the geographic locations of these Seas. They correspond to the possible sites of convection in the model, calculated with a physical threshold on the maximum of the mixed layer depth of 1,000 m for all the experiments, and of 700 m for the observation-based estimates. If in one experiment the mixed layer is deeper than this threshold, then the grid-point is selected as potential convection sites. Then we aggregate the grid-points selected in different boxes corresponding approximately to the different seas cited

possibly because the effects of processes 1, 2 and 3 compensate each other in their simulation. An additional difficulty is that the scenario response varies from one convection site to the other. Wood et al. (1999) note in an IPCC scenario with the HadCM3 model that the Labrador Sea stops convecting while the GIN Seas keep a stable deep-water formation. More recently, Hu et al. (2004) observe the same type of sensitivity with the PCM model.

These previous studies show that to improve understanding of future characteristics of the THC, we need to better understand how the different processes operate in the region of deep water formation. The convection sites need to cross some thresholds before convection is altered. These thresholds are related to the control state of the model, which thus needs to be correctly depicted. Above all, the salinity advection mechanisms and associated time scales that maintain the salinity structure are keys for understanding and validating the processes which govern the THC in the models. How they operate in different models needs to be carefully assessed to estimate which mechanisms and processes need to be properly reproduced in order to increase our confidence in future climate projections. The analysis proposed below is a first step toward these goals.

We design a set of perturbation experiments to explore the effect of global freshwater forcing on the THC in a CGCM, and to investigate how and at which minimum time scale river runoff and direct atmospheric freshwater fluxes impact the regions of deep water formation. We evaluate the impact of these two different forcings separately by setting them to zero respectively in the first two experiments. In a third one, we evaluate their impact jointly by setting all the freshwater forcings to zero. Similar experiments have been made and analyzed by Williams et al. (2006) with a focus in the low latitude of the Pacific ocean. Here we focus on the Atlantic convection sites, where the use of a CGCM allows a regional analysis. The perturbation experiments will help to highlight the influence of the global freshwater forcing on the salinity related processes 1, 2 and 3 on the THC. Associated time scales and relative impact on the different convection sites will be the key issues addressed in this study. The originality of our simulations lies in the fact that they take into account the THC sensitivity to freshwater flux for the whole globe.

The paper is organized as follows: In Sect. 2, the coupled model and the perturbation experiments are described, and the model climatology is evaluated with respect to available observations. Section 3 focuses on the analysis of the perturbation experiments and on the oceanic response in the North Atlantic, with emphasis on the convection sites and the different time scales of the oceanic mechanisms associated with processes 1, 2 and 3. A discussion and a summary conclude the paper.

2 The experimental set-up

2.1 The coupled model

The model used in this study is the version 4 of the ''Institut Pierre Simon Laplace'' (IPSL) global atmosphere-ocean-sea-ice coupled model (Marti et al. 2005). It couples the atmosphere general circulation model LMDz (Li 1999), developed at the Laboratoire de Météorologie Dynamique (LMD, IPSL) and the ocean general circulation model ORCA/OPA (Madec et al. 1998), developed at the Laboratoire d'Océanographie Dynamique et de Climatologie (LODYC, IPSL). A sea-ice model (Fichefet and Morales Maqueda 1997), which computes ice thermodynamics and dynamics, is coupled with the ocean-atmosphere model. The atmospheric model is coupled to the OR-CHIDEE land-surface model (Krinner et al. 2005). The ocean and the atmosphere exchange surface temperature, sea-ice cover, momentum, heat and freshwater fluxes once a day, using the OASIS coupler (Valcke et al. 2004) developed at the CERFACS (Centre Européen de Recherche et de Formation Avancée en Calcul Scientifique). A river routing scheme distributes the continental runoff on the appropriate coastal grid of the ocean GCM. No flux correction is applied, which is important to improve reliability of coupled processes (Neelin and Dijkstra 1995). Tziperman (2000) also pointed out that flux correction seriously impacts the non-linear effects that affect the THC. In addition, the coupling scheme ensures both global and local conservation of heat and freshwater fluxes at the model interfaces.

The model is run with a horizontal resolution of 96 points in longitude and 71 points in latitude (3.7° × 2.5°) for the atmosphere and 182 points in longitude and 149 points in latitude for the ocean, corresponding to a resolution of about 2°, with higher latitudinal resolution of 0.5° in the equatorial ocean. There are 19 vertical levels in the atmosphere and 31 levels in the ocean with the highest resolution (10 m) in the upper 150 m.

Several aspects of the ocean component are important for this study. In the northern hemisphere, the mesh has two continental poles so that the ratio of anisotropy is nearly one everywhere. This gives a good representation of the Arctic ocean and avoids numer-

ical instabilities at the pole. Vertical eddy diffusivity and viscosity coefficients are computed from a level 1.5 turbulent closure scheme based on a prognostic equation for the turbulent kinetic energy (Blanke and Delecluse 1993). The Gent and Mc Williams (1990) parametrization, with spatially varying coefficient, is used in order to represent the effects of mesoscale eddies on the transport of tracers and large-scale oceanic circulation. In locations with statically unstable stratification, a value of 100 m^2/s is assigned to the vertical eddy coefficients for momentum and tracers. A free surface is implemented (Roullet and Madec 2000) which ensures salt conservation.

2.2 Control simulation in the North Atlantic

The major features of the control simulation CTRL are documented in Marti et al. (2005). The focus here is on the formation of deep water in the North Atlantic. Except in the region around 45°N–50°W, the climate is reproduced satisfactorily in most places of the North Atlantic. Compared to Levitus (1982), SST errors are less than 2°C (Fig. 2). Freshwater forcing north of 45°N shows that the global balance is well reproduced especially for continental runoff (Table 1). Export of sea-ice in the model across the Fram Strait is about 0.1 Sv each year which is in agreement with available data (Kwok et al. 2004). The extent of sea-ice is correctly simulated, with a small eastward extent bias east of Greenland which is linked to the eastward shift of the convection sites in the model. Deep water formation sites are located in the GIN and Irminger Seas as in the estimates of mixed layer depth (Fig. 3) by de Boyer Montégut (2004). Convection in the Irminger Sea was documented in Pickart et al. (2003) but is too far east in the model compared to the observations. The same remark can be made for the convection in the GIN Seas. Part of the difference with observations is due to the fact that convection is a very complex process occurring on a scale of a few kilometers. Convection processes are not captured explicitly by the present day CGCM. Moreover, observations are smoothed when averaged on the CGCM grid, partly explaining the difference between CTRL and observations. A major drawback is the lack of convection in the Labrador Sea.

The biases observed around 45°N–50°W are likely due to a tilted representation of the Gulf Stream partially associated with the wind stress forcing. In the model, the wind structures are shifted toward the equator in mid-latitude as it is often the case in coarse resolution CGCMs. The freshwater forcing, compared to a climatology by da Silva (1994), also shows an
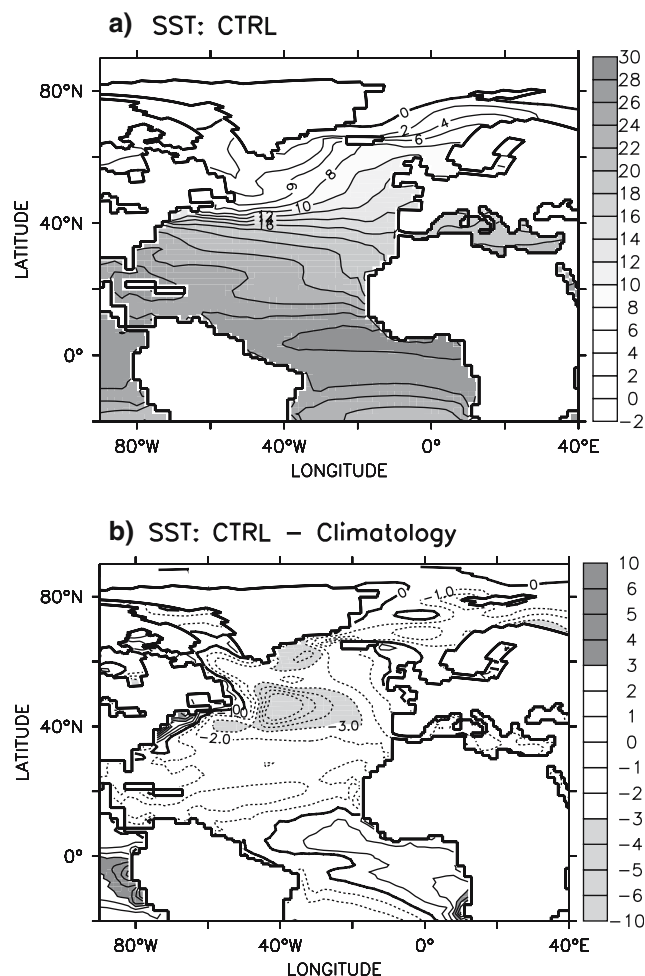

Fig. 2 a Annual mean SST for CTRL experiments and b difference with Levitus SST (1982). The contour interval is 2°C for (a) and 1°C for (b). Negative values are shown as *dashed lines*

important bias in the $E - P$ budget around 45°N–50°W (Fig. 4). This bias in $E - P$ budget results from stronger than observed precipitation (14%) and weaker evaporation (15%) which lead to a 70% error in the $E - P$ budget between 45°N and 50°N (Table 1). The SSS deficit around 45°N–50°W (Fig. 4) is associated with this stronger freshwater local forcing, with a larger westward extension due to the advection by the North Atlantic drift. These local biases affect conditions in the Labrador Sea which is positioned at the confluence of three major freshwater pathways (the West Greenland Current, the Baffin Island Current, and Hudson Straight outflow). A cold halocline (0.5 PSU/100 m in the first 400 m, not shown) appears in this sea in CTRL during the first 10 years and prevents deep water formation. In March, the halocline favors a larger than observed sea-ice cover extension which in turn reduces the heat fluxes with the atmosphere by an order of magnitude, and damps atmospheric thermal cooling.

Table 1 Comparison of the freshwater budget (in Sv) of CTRL simulation with climatology of continental runoff discharge (R) from UNESCO and evaporation minus precipitation (E – P) from da Silva (1994) for different latitude bands in the North Atlantic

Regions	North of 45°N		45°N–50°N		50°N–70°N (convection sites)		70°N–90°N (Arctic)	
Forcing	CTRL	Clim	CTRL	Clim	CTRL	Clim	CTRL	Clim
Runoff	0.19	0.18	0.04	0.04	0.07	0.10	0.08	0.04
E – P	– 0.22	– 0.14	– 0.14	– 0.04	– 0.08	– 0.10	– 1.10^{-3}	– $0.8.10^{-3}$
E	0.39	0.42	0.25	0.29	0.13	0.13	2.10^{-3}	$0.9.10^{-3}$
P	0.61	0.56	0.39	0.33	0.22	0.23	3.10^{-3}	$1.7.10^{-3}$
E – P – R	– 0.41	– 0.32	– 0.18	– 0.08	– 0.15	– 0.20	– 0.08	– 0.04

The sum E – P – R is shown in the last line. The total E – P – R bias between CTRL simulation and observations equals 0.09 Sv north of 45°N. This leads to a 0.9 Sv.decade bias if integrated over a decade
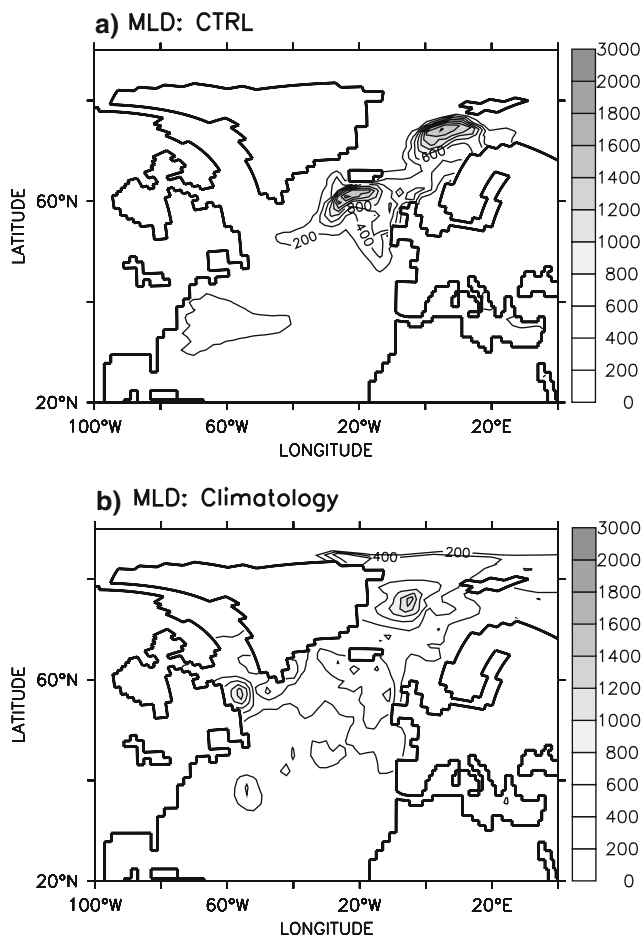
Fig. 3 March mixed layer depth in **a** CTRL averaged over years 50–100 and **b** for a climatology from de Boyer Montégut (2004). The contour interval is 200 m

We follow the approach of Walin (1982) and Tziperman (1986) to analyze the water mass transformation rates from heat and freshwater fluxes at the ocean's surface for three boxes (Fig. 1) corresponding approximately to the Labrador, the Irminger and the GIN Seas, which are potential regions of convection, as seen in Fig. 3. The transformation leads to water mass formation due to air-sea fluxes that feeds the North Atlantic deep water (NADW) and thus the THC. The thermal and haline contributions in the transformation are shown in Fig. 5 for the three regions defined before, both for CTRL and for a climatology computed from Levitus (1982) and ERA40 (Uppala et al. 2005) climatological datasets. The thermal contribution to density change dominates the haline contribution by at least an order of magnitude. This confirms that deep water is mostly produced by direct atmosphere cooling (Speer and Tziperman 1992). In the GIN and Irminger Seas, transformation amplitudes are rather satisfactory with a maximum of 4 Sv in the GIN Seas and 8 Sv in the Irminger Sea very close to observation-based estimates (Fig. 5). In the Labrador Sea, there is almost no transformation of dense water in CTRL compared to climatology, confirming the absence of convection.

The lack of convection in the Labrador Sea seems to be the reason why the THC strength is only 10–12 Sv (Fig. 6a). That is slightly weaker than observation-based estimates which evaluate the production of NADW to 15 ± 2 Sv (Ganachaud and Wunsch 2000). Indeed, the outflow of water denser than 27.8 kg/m^3 over the GIS ridge (GIN Seas outflows) is of 5.4 Sv in CTRL, compared with observational estimates of 5.6 Sv (Dickson et al. 1994), which suggests that the circulation is correct in this region.

2.3 Description of the perturbation experiments

The perturbation experiments are designed to destabilize the system in order to understand how the global freshwater forcing maintains the salinity structure and influences the salinity transport, with a focus on the way the three convection sites are affected, including their associated time scales. The perturbation experiments consist of switching off some forcing terms of the salinity field in the ocean model during the coupling

Fig. 4 **a** CTRL SSS and **b**
$E - P$ pattern averaged over
years 50–100 and difference
between CTRL and
climatology for **c** SSS (Levitus
1982) and **d** $E - P$ (da Silva
1994). The contour interval is
0.5 PSU for (**a**) and (**c**),
1 mm/day for (**b**) and (**d**).
Negative values are shown as
dashed lines
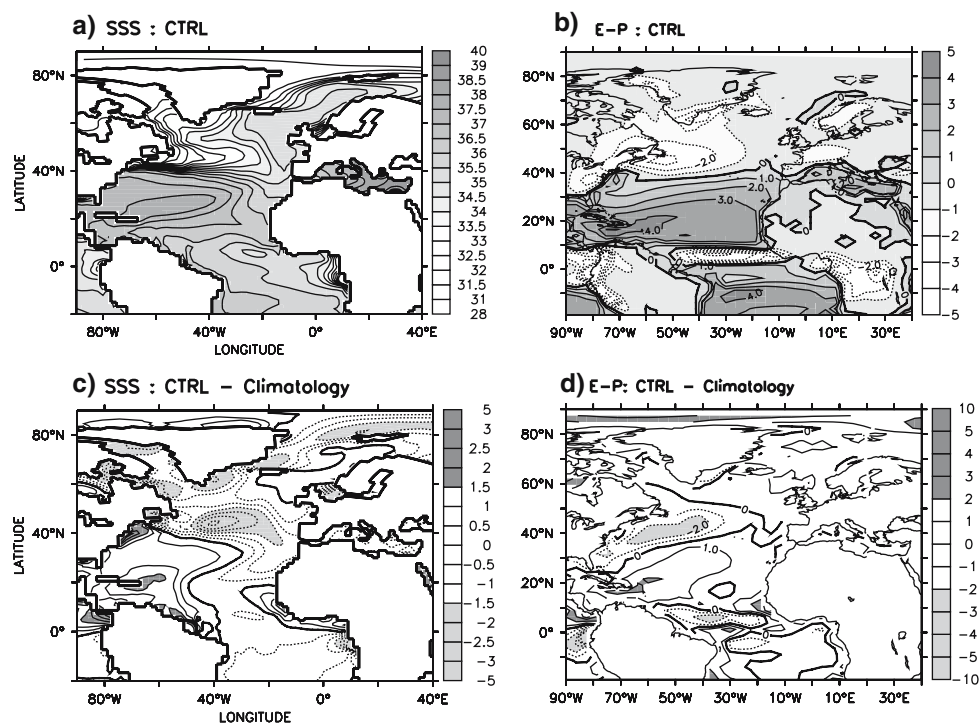
procedure. The equation of conservation of salinity used in the ocean model is:

$$\frac{\partial S}{\partial t} = \mathrm{Adv}(S) + Diff(S) + S(E - P - R + G)\delta(z - \eta) \tag{1}$$

where S corresponds to salinity, $Adv()$ is the function of advection for the tracers, $Diff()$ the function related to diffusion, $\delta()$ the Dirac function, z the vertical coordinate, t the time, η the height of the free surface. In this equation, E corresponds to evaporation, P to precipitation, R to runoff and G to the sea-ice freshwater exchange that could be positive (brine rejection) or negative (ice melting).

In order to separate the influence of the direct freshwater atmospheric forcing ($E - P$) from the continental runoff (R), three different experiments have been performed. In the first one (EP0) we prescribe the term $E - P$ to zero. This is done globally by replacing at each ocean grid-point and at each time step the values coming from the atmosphere model by zero. The second one (R0) attempts to isolate the influence of the continental runoff. It is done following the same procedure, by prescribing R to zero. In the last one (EPR0) all the freshwater fluxes, except the one associated with sea-ice, are set to zero ($E - P - R = 0$). An additional test ($G = 0$, not considered here) confirmed that sea-ice freshwater fluxes have a second order

effect on the Atlantic THC (Goosse and Fichefet 1999). The equation for the ocean temperature is not affected in any of these experiments, and at each time step the atmosphere normally computes surface fluxes using ocean simulated SST. Note that this methodology ensures the thermal energy conservation in each experiment.

All these experiments start from Levitus (1982) as for the control simulation (CTRL). Initial conditions for the atmosphere are derived from an observed 1 January, and the sea-ice starts from a 1 January from a balanced ocean sea-ice simulation forced by NCEP reanalysis. Experiments are integrated for 100 years in order to investigate how salinity field and deep water formation are affected under a time frame compatible with climate projection for the next century.
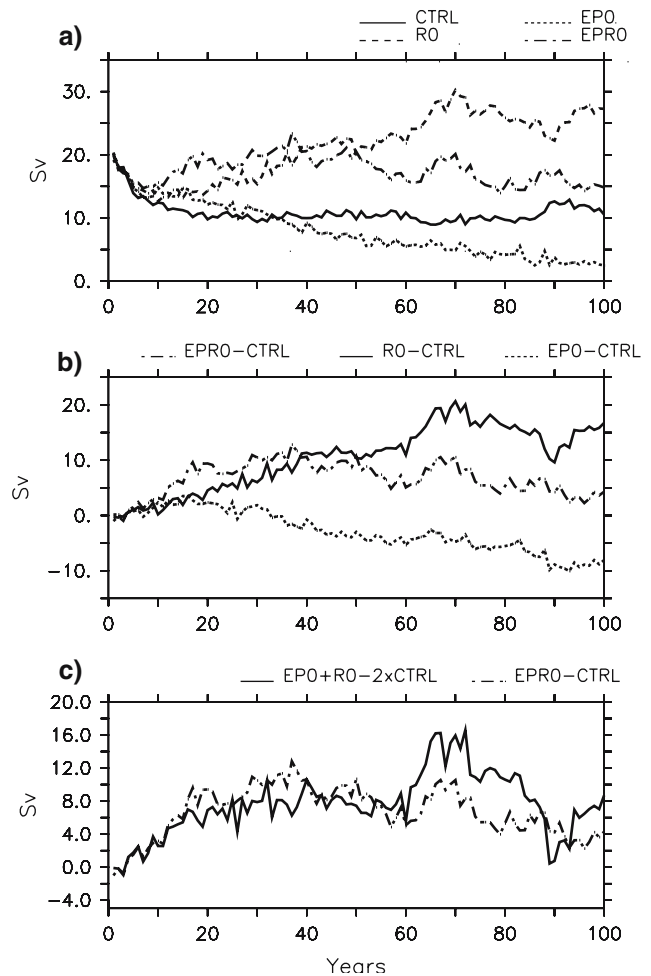
3 Impact of modified freshwater forcing

3.1 THC and water mass transformation response

Figure 6a shows the response of the THC index for all experiments. Each sensitivity experiment exhibits the same THC decrease as CTRL in the first 10 years, which suggests a common adjustment among the experiments, corresponding to the fast dynamical adjustments of the upper ocean to the atmosphere when coupled. After this period, comparison of the
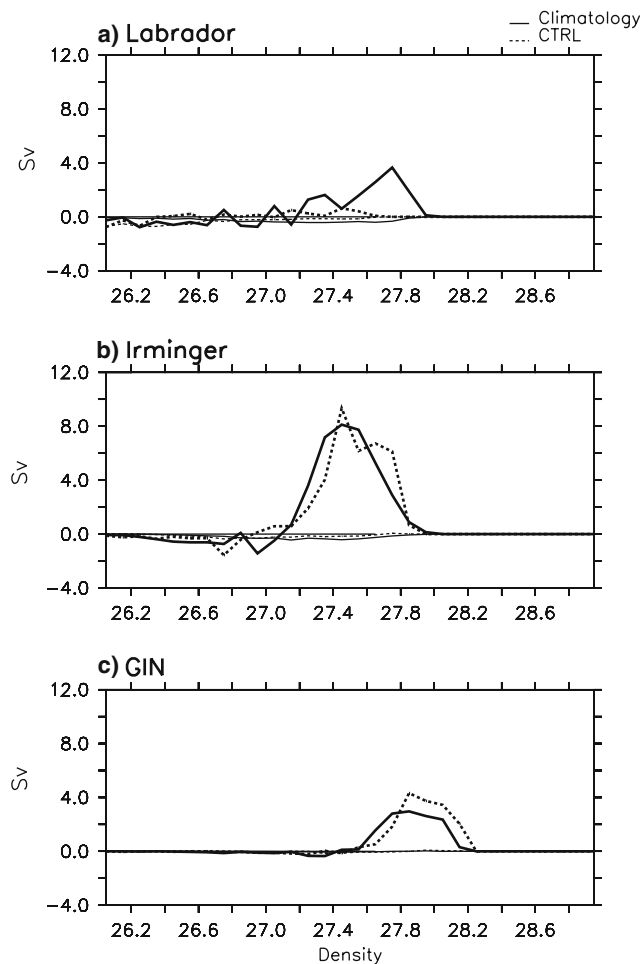
Fig. 5 Transformation of water mass (in Sv) for the three different convection sites. The *solid lines* stands for the climatology and the dotted lines for the CTRL experiment averaged last 50 years. The *heavy lines* represents the thermal contribution to the transformation and the thin line the haline contribution. **a** Labrador Sea. **b** Iminger Sea. **c** Gin Seas. Air–sea exchange of heat and freshwater continuously transforms the characteristics of the surface waters from one density class to another. A positive value of the transformation stands for a transformation of water mass toward higher density and vice versa

Fig. 6 The THC index is defined as the maximum of the Atlantic meridional overturning circulation between 500 and 5,000 m depth (Manabe and Stouffer 1999). **a** THC index for the CTRL (*solid line*), EPR0 (*dash–dotted line*), EP0 (*dotted line*) and R0 (*dashed line*). **b** Difference of each experiment with CTRL, R0–CTRL in *solid line*, EP0–CTRL in *dotted line*, EPR0–CTRL in *dash–dotted line*. **c** EPR0–CTRL (*solid line*) and EP0 + R0 – 2 × CTRL (*dash–dotted line*)

THC index between the sensitivity experiment and CTRL (Fig. 6b) reflects the impact of the modified freshwater forcing on the THC. The index increases in R0 for the first 70 years and then stabilizes around 25 Sv, whereas in EP0 it decreases throughout the simulation to reach 3 Sv after 100 years. The behavior is more complex in EPR0. It increases for the first 30 years and then slowly decreases. Figure 6c shows that the response of EPR0, during the first 60 years, is nearly the sum of EP0 and R0 responses. Given that the freshwater perturbation of EPR0 is the sum of the perturbations in EP0 and R0, this means that the system responds quasi-linearly during the first 60 years. A

similar result was found by Dixon et al. (1999) although the thermal and haline forcings were different in their experiments. This linearity will be used to explain the behavior of EPR0 with respect to R0 and EP0 responses.
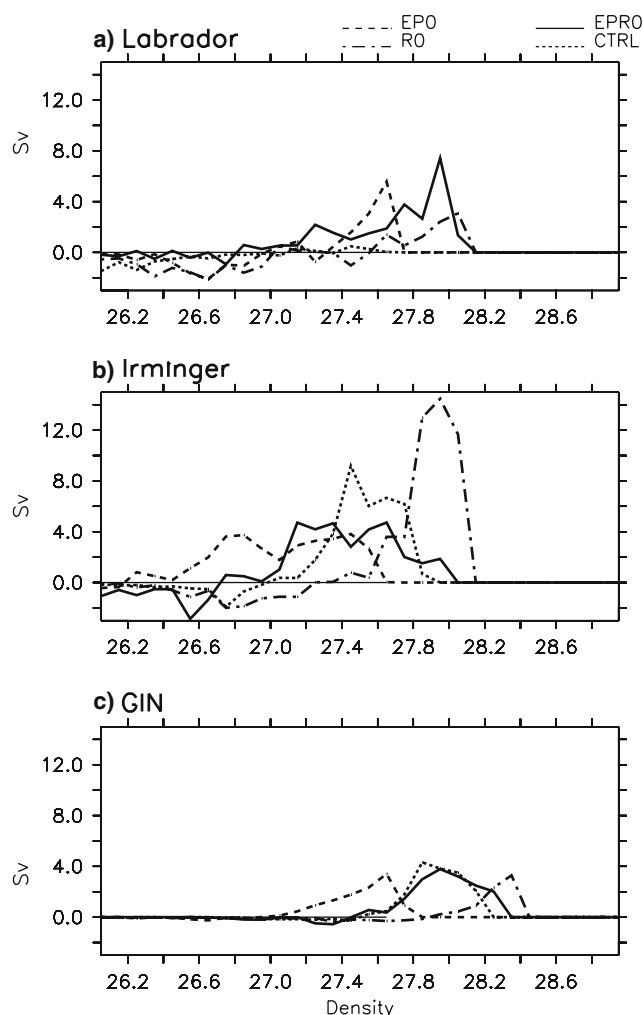
Figure 7 shows for each experiment, using an average over the last 50 years, how the mixed layer depth has changed in the North Atlantic compared to CTRL. Convection increases in the Labrador Sea when freshwater fluxes are not active (EPR0) and decreases in the Irminger Sea. When only $E - P$ is removed (EP0), convection vanishes almost everywhere, whereas it remains active in most of the North Atlantic when only runoff is removed (R0).
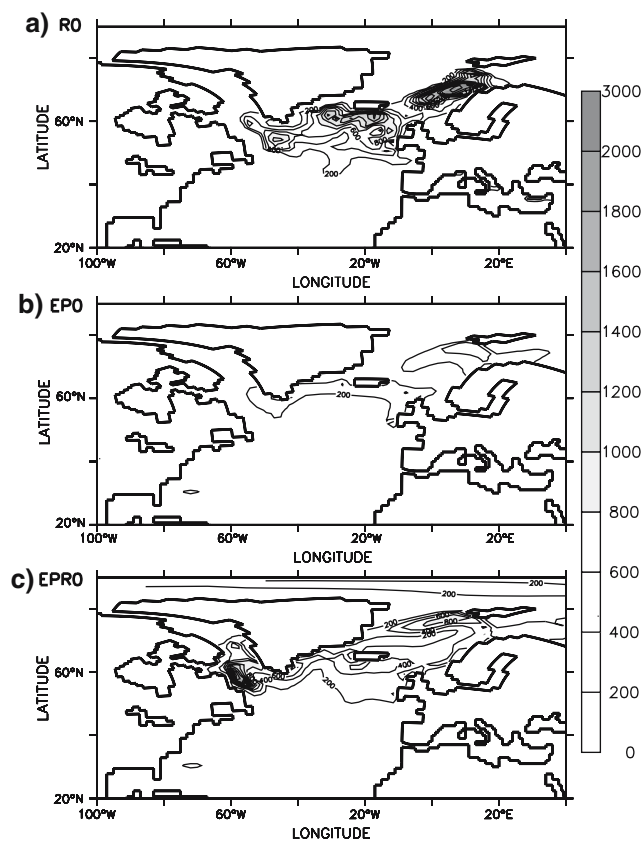
Fig. 7 March mixed layer depth averaged over the last 50 years for the different perturbation experiments. **a** R0. **b** EP0. **c** EPR0. The contour interval is 200 m

Fig. 8 Same as Fig. 5, with in *solid line* experiment EPR0, in *dotted line* the CTRL, in *dash–dotted line* R0 and in *dashed line* EP0, averaged over the last 50 years

To further investigate changes in the convection sites, water mass transformation by the air–sea fluxes has been calculated (cf. Sect. 2) for each site. In the GIN Seas (Fig. 8c), water mass transformation in EPR0 remains comparable to CTRL. Transformation is switched toward higher density in R0 and lower density in EP0, by the same amount of 4 Sv in both experiments. This means that less dense water is formed in EP0 and more dense water in R0, which is in qualitative agreement with the mixed layer analysis. EPR0 transformation is in the middle of EP0 and R0 transformation, which may result from compensation between the effect of runoff and surface E – P fluxes. Thus, the GIN Seas seem to be little affected by changes in global freshwater fluxes.

In the Irminger Sea (Fig. 8b), we observe an important increase of transformation of water denser than 27.8 kg/m^3 in R0 with more than 14 Sv of water transformed around density 28 kg/m^3. In EP0 on the contrary, water class transformation is spread and shifted toward water lighter than 27.6 kg/m^3. In EPR0 we observe a spreading of the transformation and a diminution of the maximum, so that, compared to

CTRL, less water between 27.3 and 27.8 kg/m^3 is transformed and more water in the class higher than 27.9 kg/m^3 or smaller than 27.2 kg/m^3 is transformed.

In the Labrador Sea (Fig. 8a), the occurrence of convection is linked to some positive water transformations in the three perturbation experiments. The transformation concerns water between 27.4 and 27.8 kg/m^3 in EP0 with a maximum of 5 Sv, and water denser than 28 kg/m^3 in R0 with a maximum of 3 Sv. In EPR0, we observe a vigorous transformation (7 Sv) of water denser than 27.8 kg/m^3. This transformation is associated with the absence of sea-ice cover in March in the Labrador Sea (not shown).

3.2 Changes in freshwater transport

Change in the THC triggers a negative temperature related feedback. When the THC strengthens (re-

duces) the meridional northward heat transport strengthens (reduces). Temperature changes are thus observed together with salinity changes in the convection sites in the different experiments. The respective contributions of salinity and temperature anomalies on the density stratification have been calculated (not shown) and reveal that changes in salinity are the dominant factor in our simulations.

Salinity in the convection sites depends on the salinity transport and on the local freshwater forcing, whereas diffusion is negligible (not shown). This salinity transport is evaluated through the freshwater transport, defined as:

$$F_t = -v \frac{(S - S_0)}{S_0} dx \, dz \qquad (2)$$

where v is the northward velocity, and S_0 is a reference salinity equal to 34.9 (mean salinity of the Atlantic ocean). This definition follows Wijffels et al. (1992) approach. Here, it represents the difference between the mass transport and the salt transport divided by a reference salinity, in order to express F_t in Sverdrups. This is based on the hypothesis of salt conservation, and is thus well adapted to our free surface Ocean GCM. It is a generalization of the overturning freshwater definition in Lohmann (2003). It expresses the whole effect of salinity advection with respect to a reference salinity. In steady state F_t is in balance with the meridionally integrated freshwater forcing, so that this transport is a measure of the advective adjustment to changes in the surface freshwater forcing. One can define an overturning (zonal mean) component and a gyre (zonal anomaly) component (Wijffels 1992) that will help to identify the role of both components in CTRL simulation (Fig. 9). Both components contribute to about half of the total transport F_t. A climatology of the freshwater transport has been evaluated following Wijffels et al. (1992): the ocean freshwater forcing climatology by da Silva (1994) has been meridionally integrated, so that it expresses an indirect freshwater transport estimate, with a reference transport equal to the model's one at 30°S. Considering the fact that this type of evaluation has a large error (60% at 30°S, if integrated from the Bering Strait according to Wijffels et al. 1992), we can say that the latitudinal variations in the freshwater transport is correctly simulated, and that the bias in the freshwater balance (Table 1) partly explains the bias in the amplitude north of 45°N.

In the following, we will consider gyre and overturning together (F_t) because they participate together in the advective adjustment. If F_t is negative (positive),
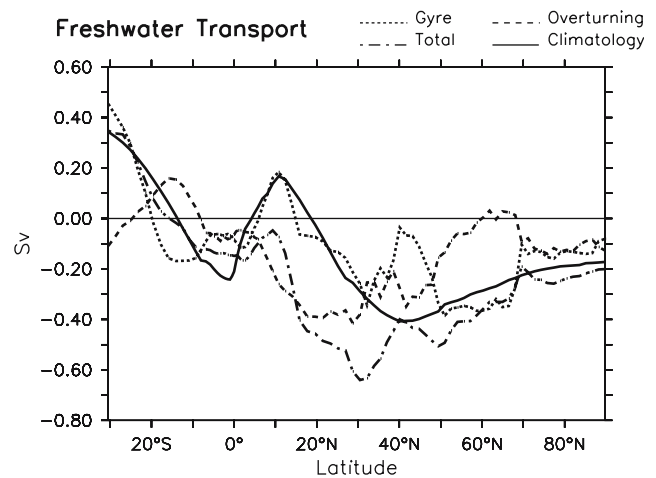
Fig. 9 Meridional freshwater transport in the Atlantic with respect to a reference salinity. The *solid line* represents a climatology, the *dash–dotted line* the CTRL, the *dotted line* the gyre component for CTRL, and the *dashed line* the overturning component for CTRL

the transport of freshwater is southward (northward) and thus the salinity transport with respect to a reference salinity is northward (southward). Between 10°S and 50°N, the northward salinity transport corresponds to Nsa, whereas between 70°N and 90°N, the southward freshwater transport corresponds to Ssa.

We further verify that the anomalies in salinity transport in EPR0 are not due to some significant changes in the circulation but mostly to the salinity changes. We decompose salinity as: $S = \Delta S + S^{CTRL}$ where ΔS represents the anomaly compared to CTRL, and S^{CTRL} is the salinity of CTRL, and similarly for the meridional northward velocity: $v = \Delta v + v^{CTRL}$. This leads to the following decomposition of F_t:

$$\underbrace{\Delta F_t}_{(a)} = \underbrace{-\frac{1}{S_0} v^{CTRL} \Delta S dx \, dz}_{(b)}$$
$$\underbrace{-\frac{1}{S_0} \Delta v (\Delta S + S^{CTRL} - S_0) dx \, dz}_{(c)} \qquad (3)$$

Term (a) corresponds to the difference in the freshwater transport between the perturbed experiments and CTRL. (b) stands for the transport of salinity anomalies, while (c) corresponds to the changes in circulation.

Figure 10 shows these three components for EPR0. The transport of the salinity anomalies is the major component of the freshwater transport anomalies. The change of circulation is less important, only playing a role between years 10 and 40, when the THC increases
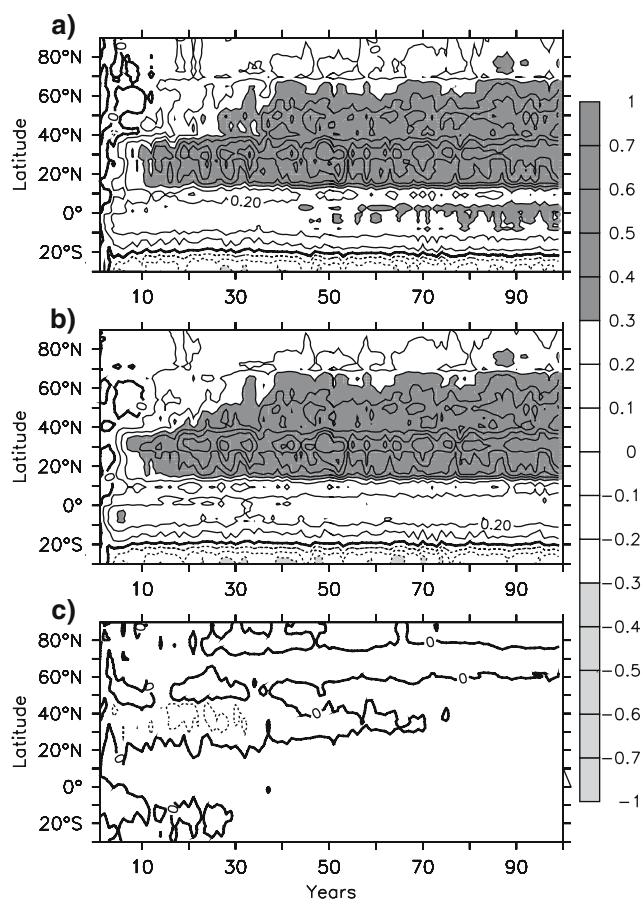
Fig. 10 Time-latitude diagram of the decomposition of the meridional freshwater transport anomaly between EPR0 and CTRL in the Atlantic. **a** ΔF_{ot}. **b** $-\frac{1}{S_0}\int_{-h}^{0}v^{\mathrm{CTRL}}\Delta S dz$. **c** $-\frac{1}{S_0}\int_{-h}^{0}\Delta v(\Delta S + S^{\mathrm{CTRL}} - S_0)dz$. The contour interval is 0.1 Sv. Negative values are shown as *dashed lines*

in EPR0, enhancing the meridional velocity and thus the transport. This process was described by Stommel (1961) as a positive feedback of salinity transport on the THC. In Fig. 10a, we observe that freshwater transport diminishes in EPR0 compared to CTRL. This is explained by the homogenization of salinity distribution, due to the absence of freshwater forcing. Between 10°S and 50°N evaporation dominates in CTRL. This band of latitude becomes fresher in EPR0, so that the Nsa decreases. Thus the Nsa is divided by two in 30 years, and has totally disappeared in 60 years, leading to a decrease of the salinity transport to the convection sites. Between 70°N and 90°N, the same phenomenon occurs: Ssa is divided by two, but the time scale is only 10 years and it vanishes in 20 years. This leads to a decrease of the associated freshening in the convection sites.

Since our experimental design implies global freshwater forcing changes, modification at the boundaries of our study domain at the Bering Strait and 30°S could

play a role. These terms are however of second order for the salinity balance (not shown), and their role is thus negligible in comparison with perturbation over the Atlantic. Two different time scales appear in this analysis: a rapid one linked to Ssa (10 years), and a slower one linked to Nsa (30 years). Ssa transports a positive salinity anomaly in all perturbed simulations, whereas Nsa transports a negative salinity anomaly in EP0 and EPR0 and a positive one in R0. With these remarks in mind, we will analyze in more detail how Nsa and Ssa affect the different convection sites.

3.3 Changes in the convection sites mean stratification

Figures 11, 12 and 13 show the mean density anomalies at each site for each experiment. These anomalies are mostly driven by salinity advection (not shown) associated with salinity changes in remote areas.

3.3.1 The Labrador Sea

In the Labrador Sea, analysis of R0 shows that a 0.2 kg/m³ positive surface density anomaly, driven by salinity, appears after 10 years (Fig. 11a). However, it takes 35 years to destabilize the water column, and to increase the mixed layer depth by more than 500 m. The latter occurs when a threshold anomaly of 0.5 kg/m³ is reached in the first 500 m. Note that the value is larger at the surface (1 kg/m³) and vanishes at 500 m. A simple dilution model applied to the Labrador Sea allows this threshold to be related to a surface freshwater forcing of 0.6 Sv.decade. This value is lower than the 0.9 Sv.decade integrated E – P – R bias of the CTRL compared to observation-based estimates north of 45°N (Table 1). This means that part of the E – P – R bias north of 45°N, integrated over 10 years, is a good candidate to explain the halocline bias observed in CTRL, in the Labrador Sea.

In EP0 (Fig. 11b), a positive salinity driven density anomaly appears immediately in the first 500 m. The anomaly increases nearly linearly at the surface for the first 20 years so that a growth rate of 0.14 kg/m³/decade can be estimated from a linear regression, calculated on the mean anomaly of the first 500 m (Fig. 11d). After 20 years the anomaly stabilizes, and then decreases with a 0.08 kg/m³/decade negative growth rate calculated from year 30 to 100. The initial positive trend is then counteracted by a negative anomaly. EPR0 results from the combination of the three effects. The water column is destabilized immediately with a growth rate of 0.18 kg/m³/decade. After 10 years this growth rate increases to 0.27 kg/m³/dec-
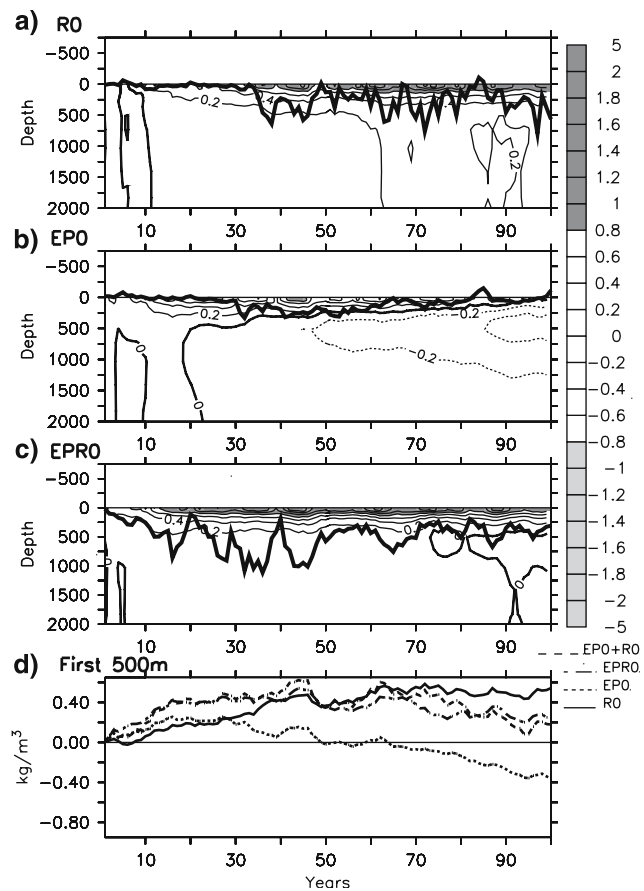
Fig. 11 Time-depth difference in density with the CTRL simulation for the Labrador Sea. **a** R0. **b** EP0. **c** EPR0. The *heavy solid line* corresponds to the mixed layer depth anomaly in March compared to CTRL simulation. The contour interval is 0.2 kg/m^3. In **d** are plotted the first 500 m averaged density anomaly for the three experiments and for the sum of EP0 and R0

ade (Fig. 11c). During the first part of the simulation, this approximately corresponds to the sum of the growth rates in EP0 (0.15 kg/m^3/decade) and in R0 (0.08 kg/m^3/decade) after 10 years. After year 20, the anomaly stabilizes as in EP0 and from year 45, a decrease of the anomaly, as well as a decrease of the mixed layer depth, is observed with a 0.02 kg/m^3/decade negative growth rate. The mixed layer remains deeper than in CTRL throughout the EPR0 simulation. This analysis shows that local forcing and Ssa dominate the impact on stratification during the whole 100 years in the Labrador Sea.

3.3.2 The Irminger Sea

In the Irminger Sea, the mixed layer is deeper in R0 than in CTRL after 10 years (Fig. 12a), resulting from a positive salinity driven density anomaly in the first 500 m. This anomaly has a growth rate of 0.05 kg/m^3/
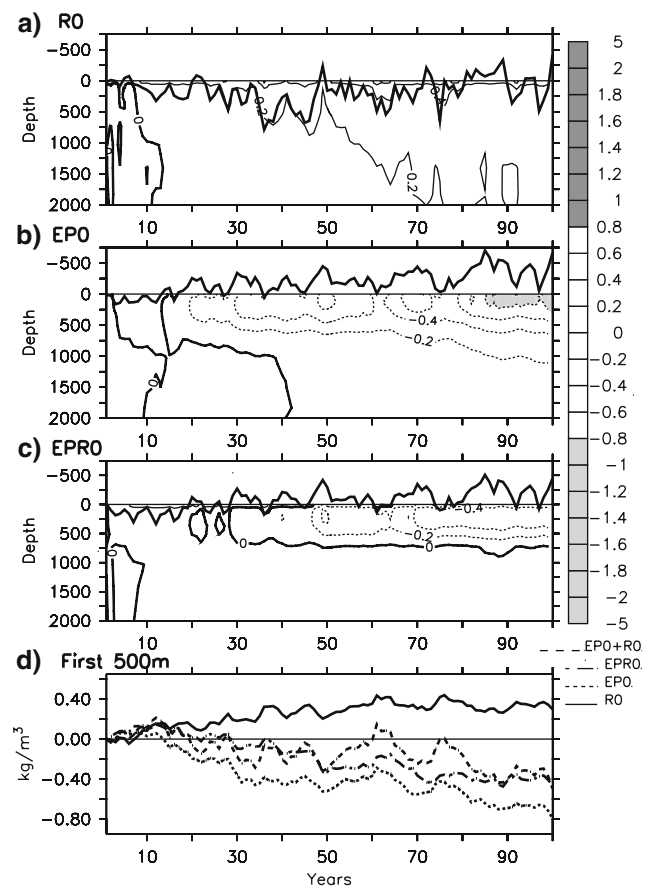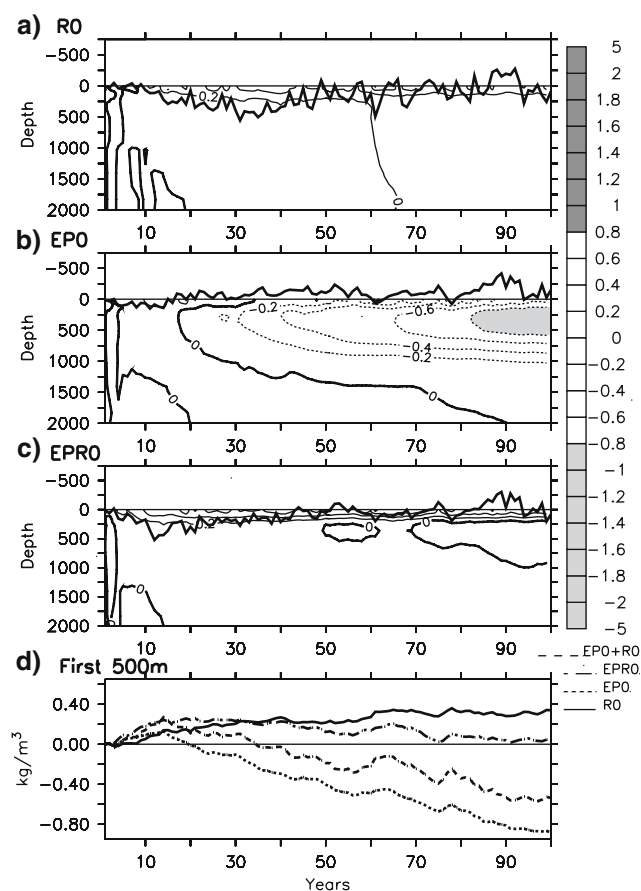
Fig. 12 Same as Fig. 11 but for the Irminger Sea

decade. In EP0 (Fig. 12b), the opposite is true. After 15 years, the water column begins to be stabilized by a negative salinity anomaly with a negative growth rate of 0.12 kg/m^3/decade. In EPR0 (Fig. 12c), a positive anomaly appears for the first 15 years with a 0.07 kg/m^3/decade growth rate. Then the anomaly stabilizes at year 15, and decreases with a 0.06 kg/m^3/decade negative growth rate, so that after year 30 the anomaly becomes negative as does the mixed layer depth anomaly. Once more the two signals found in EP0 and R0 nearly add up (Fig. 12d). This sea is mostly sensitive to the Nsa influence.

3.3.3 The GIN Seas

In the GIN Seas, the mixed layer deepens in R0 (Fig. 13a) after 10 years, associated with a positive salinity driven density anomaly with a growth rate of 0.05 kg/m^3/decade. In EP0, a positive anomaly is seen for the first 20 years, with a growth rate of 0.06 kg/m^3/decade (Fig. 13b). After year 20, a negative anomaly appears, with a growth rate of 0.10 kg/m^3/decade, illustrating the impact of the reduced Nsa. In EPR0

Fig. 13 Same Fig. 11 but for the GIN Seas

Table 2 Sensitivity of the three convection sites to freshwater advection, based on an analysis of the convection sites' stratification in the different perturbation experiments

	Labrador Sea	Irminger Sea	GIN Seas
Nsa	+(30 years)	+(15 years)	+(20 years)
Ssa	– (10 years)	– (10 years)	– (10 years)
Global	–	+	/

Nsa (Ssa) corresponds to Northward (Southward) salinity advection. The sign – means that the process limits convection, the sign + that it enhances convection and the sign/stands for neutral impact. The time scale needed for the process to impact upon the region (changes in the trend of the stratification anomaly in the first 500 m) after a modification of the freshwater forcing in the source region is indicated in parentheses. The ''Global'' lines gives an idea of which processes dominates after 50 years

ocean were set to zero (R0); in the second one, $E - P$ fluxes were set to zero (EP0) and in the last one, $E - P$ and runoff were removed (EPR0). Sensitivity of the North Atlantic deep convection sites (Labrador, Irminger and GIN Seas) to these global changes in freshwater forcing is our focus. These extreme experiments are designed to evaluate the relative strength of salinity driving processes, with their associated time scales. We considered in particular the local adjustment of the water column in the different convection sites as well as the role of the southward transport of freshwater from the Arctic (Ssa), and the northward salinity advection (Nsa), notably from the tropics, toward the convection sites. In all the perturbation experiments, temperature has only a second order effect on the stratification changes in the convection sites. Ssa, local freshwater forcing and Nsa have dominant contributions to the adjustment of the convection sites.

From our results using the IPSL-CM4 model, it is shown that (Table 2):

- The Labrador Sea, which is not a convective site in CTRL, is very sensitive to local freshwater fluxes and Ssa;
- The Irminger Sea is mainly sensitive to Nsa;
- The Gin Seas are sensitive to Ssa, local forcing and Nsa with nearly the same magnitude.

The difference of sensitivity between the Labrador and GIN and Irminger Seas is similar to that found by Wood et al. (1999) in an IPCC scenario. In their experiment, the Labrador convection site rapidly collapses due to an increase of local freshwater forcing, while in the Irminger and GIN Seas convection remains the same, because Nsa increases and destabilizes these sites. According to our perturbation experiments, the Labrador Sea is also very sensitive to freshwater

(Fig. 13c) there is a positive salinity driven density anomaly with a growth rate of 0.13 kg/m^3/decade for the first 20 years, and then a negative anomaly, with a growth rate of 0.03 kg/m^3/decade, stabilizes the water column. This Sea shows a less linear behavior (Fig. 13d). The mixed layer deepens during the first 20 years (Fig. 13c) and then comes back to the level of CTRL after 50 years.

The sensitivity of each site to the processes Nsa and Ssa and their associated time scales is summarized in Table 2. It is deduced from freshwater transport evolution and stratification timing analysis.

4 Discussion and conclusions

In this study, the sensitivity of the THC to global freshwater forcing over a century has been assessed. For this purpose the ocean system was destabilized through perturbation experiments, using the IPSL-CM4 coupled GCM, a state-of-the art coupled model, with a closed freshwater budget in the control simulation. In a first experiment, runoff fluxes toward the

forcing in the IPSL-CM4 model, confirming the sensitivity of this Sea also found in Hu et al. (2004).

The minimum time scales associated with the different processes and observed in our perturbation experiments are not synchronous and affect the North Atlantic convection sites differently. From our analysis of the convection sites density changes and freshwater transport modification, we can deduce the following explanation for the dynamics taking place in the perturbation experiments: the local freshwater forcing impacts the convection sites with a short time scale of 1 or 2 years. Ssa, mostly associated with runoff from the Arctic, reaches all sites in about 10 years. Changes in the tropics and in the mid-latitudes influence convection sites through Nsa process in 15 years for the Irminger Sea, 20 years for the Gin Seas, and 30 years for the Labrador Sea. These different time scales are of importance for the THC, because a change in moisture transport will affect global freshwater forcing within a few years, but advective time scales may delay the THC response. Such time scales may also play an important role on the THC variability, but this is beyond the scope of this study.

The evolution of the THC for the different experiments (Fig. 6) is closely linked to these different time scales. In particular, the THC decrease in EP0 after 15 years results from the weakening of Nsa compared to CTRL that is not compensated by sufficient changes in Ssa or local forcing. Convection sites are stabilized and the THC decreases. In R0 on the other hand, an increase of surface salinity appears in most convection sites after 10 years, destabilizing them and thereby increasing the THC. In EPR0, both effects oppose each other with their own time scales. During the first 30 years, the increase of Ssa and the absence of local freshwater forcing contribute to the destabilization of the convection sites, enhancing the THC. After 30 years the weakening of Nsa starts to stabilize the water column in the convection sites, leading to the decrease of the THC, which however stays larger than in CTRL over a century.

We deduce from this analysis that over the time scale of a century, global freshwater forcing *damps* the THC. The Atlantic is an evaporative basin in CTRL, but high latitude freshening is dominant against Nsa. Consequently the THC is more sensitive to high latitude freshening than to tropical salinity forcing in this model, since the absence of freshwater forcing actually boosts the THC for the whole century. This is not in agreement with another study by Saenko et al. (2002), certainly due to the different time scales considered. Saenko et al. were interested in the ocean steady state, which means an adjustment of 1,000 years at least. Here we are interested by the transient phase and we have investigated a century long adjustment, which corresponds to the relevant time scale for future climate projections. Vellinga et al. (2002) find a time scale of THC recovery of 50 years with the HadCM3 model. This recovery was mostly due to the advection of saltier water from the tropics due to a southward shift of the Atlantic ITCZ. This time scale is longer than the one found in our experiments for Nsa, but it takes into account not only the advection, but also the atmosphere response. Moreover in the Vellinga et al. experiment, the initial state was taken to have a THC equal to zero. This must have slowed down the effect of northward advection and could explain the 50 years time scale found in their analysis, compared to our 30 years.

Understanding the convection sensitivity in our model, is also useful to provide guidance for improving model biases. We have shown that in this model, the Labrador Sea exhibits a binary behavior associated with a local positive feedback: if convection occurs, it drains water from the Gulf Stream which results in a net input of heat that limits sea-ice formation, thus enhancing convection. This positive feedback associated with sea-ice cover is linked to the existence of a threshold on stratification: either convection is possible and fed by a positive feedback or on the contrary, if the stratification is such that convection does not occur, the sea-ice cover further prevents the convection. In our model, the freshwater forcing bias observed in the CTRL inhibits convection in the Labrador Sea. An increase of density of 0.5 kg/m^3 in the first 500 m is necessary to overcome the stability threshold and allow convection. Our results also confirm that even if haline transformation is of second order compared to thermal transformation, salinity plays a crucial role in stratification over the convection sites, and thus on the preconditioning of the water.

Identifying thresholds and time scales that act in control simulations are crucial to understand how coupled GCMs work. The magnitude of our anomaly can be compared with the "water hosing" experiment of the CMIP/PMIP2 project (Stouffer et al. 2006). In EPR0 the global freshwater anomaly is equal to zero, but in the whole Atlantic the anomaly equals 0.37 Sv. It is of the same order as the 0.1 Sv and 1 Sv anomalies of the "water hosing" experiment. Our experimental design is however different since our perturbation is global. It could thus be seen as complementary to "water hosing" experiments, diagnosing the effect of the global freshwater forcing for the THC.

Our results may be model dependent especially for the time scales. Some similar studies with other models are necessary to find if the results are robust. The

analysis of other regions are also of great interest to understand the salinity related dynamics (Williams et al. (2006). Our perturbation experiments thus provide a framework for studying the salinity related processes in coupled GCM and assessing the associated time scales. This will help understand the dominant mechanism processes leading to THC changes in state-of-the-art coupled GCMs, and provide guidance for model improvement.

References

Blanke B, Delecluse P (1993) Variability of the tropical Atlantic ocean simulated by a general circulation model with two different mixed layer physics. J Phys Oceanogr 23:1363–1388

de Boyer Montégut C, Madec G, Fischer AS, Lazar A, Iudicone D (2004) Mixed layer depth over the global ocean: an examination of profile data and a profile-based climatology. J Geophys Res 109:C12003

Broecker WS (1991) The great conveyor belt. Oceanography 4:79–89

Dickson RR, Brown R (1994) The production of North Atlantic deep-water—sources, rates and pathways. J Geophys Res 12:319–341

Dixon KW, Delworth TL, Spelman MJ, Stouffer RJ (1999) The influence of transient surface fluxes on North Atlantic overturning in a coupled gcm climate change experiment. Geophys Res Lett 26:2749–2752

Fichefet T, Morales Maqueda MA (1997) Sensitivity of a global sea ice model to the treatment of ice thermodynamics and dynamics. J Geophys Res 102:12609–12646

Ganachaud A, Wunsch C (2000) Improved estimates of global ocean circulation, heat transport and mixing from hydrographic data. Nature 408:453–457

Gent PR, Mc Williams JC (1990) Isopycnal mixing in ocean circulation models. J Phys Oceanogr 20:150–155

Goosse H, Fichefet T (1999) Importance of ice–ocean interactions for the global ocean circulation: a model study. J Phys Oceanogr 23:337–355

Hu AX, Meehl GA, Washington WM, Dai AG (2004) Response of the Atlantic thermohaline circulation to increased atmospheric CO_2 in a coupled model. J Clim 17:4267–4279

Intergovernmental Panel on Climate Change (IPCC) (2001) Third assessment report of climate change, chapter 8. Cambridge University Press, London

Krinner G, Viovy N, de Noblet-Ducoudre N, Ogee J, Polcher J, Friedlingstein P, Ciais P, Sitch S, Prentice IC (2005) A dynamic global vegetation model for studies of the coupled atmosphere–biosphere system. Global Biogeochem Cycles 19:GB1015

Kwok R, Cunningham GF, Pang SS (2004) Fram Strait sea ice outflow. J Geophys Res 109:1029–1043

Latif M, Roeckner E, Mikolajewicz U, Voss R (2000) Tropical stabilisation of the thermohaline circulation in a greenhouse warming simulation. J Clim 13:1809–1813

Levitus S (1982) Climatological atlas of the world ocean. Professional paper, NOAA/GFDL

Li ZX (1999) Ensemble atmospheric GCM simulation of climate interannual variability from 1979 to 1994. J Clim 12:986–1001

Lohmann G (2003) Atmospheric and oceanic freshwater transport during weak atlantic overturning circulation. Tellus 55A:438–449

Madec G, Delecluse P, Imbard M, Lévy C (1998) OPA version 8. Ocean general circulation model reference manual. Rapp. Int., LODYC, France, 200 pp

Manabe S, Stouffer RJ (1999) The role of thermohaline circulation in climate. Tellus 51:91–109

Marti O, Braconnot P, Bellier J, Benshila R, Bony S, Brockmann P, Cadule P, Caubel A, Denvil S, Dufresne JL, Fairhead L, Filiberti M-A, Foujols M-A, Fichefet T, Friedlingstein P, Grandpeix J-Y, Hourdin F, Krinner G, Lévy C, Madec G, Musat I, de Noblet N, Polcher J, Talandier C (2005) The new IPSL climate system model: IPSL-CM4. Note du pôle de modélisation n°26. ISSN 1288-1619, 88 pp, http://www.dods.ipsl.jussieu.fr/omamce/IPSLCM4/DocIPSLCM4/

Mikolajewicz U, Voss R (2000) The role of the individual air-sea flux components in CO_2-induced changes of the ocean's circulation and climate. Clim Dyn 16:627–642

Neelin JD, Dijkstra HA (1995) Coupled ocean–atmosphere interaction and the tropical climatology, part I: The dangers of flux-correction. J Clim 8:1343–1359

Pickart RS, Spall MA, Ribergaard MH, Moore GWK, Milliff RF (2003) Deep convection in the Irminger Sea forced by the Greenland tip jet. Nature 424:152–156

Rahmstorf S, Ganopolski A (1999) Long-term global warming scenarios computed with an efficient coupled climate model. Clim Change 43:353–367

Roullet G, Madec G (2000) Salt conservation, free surface and varying levels: a new formulation for ocean general circulation models. J Geophys Res 23:927–942

Saenko OA, Gregory JM, Weaver AJ, Eby M (2002) Distinguishing the influence of heat, freshwater, and momentum fluxes on ocean circulation and climate. J Clim 15:3686–3697

da Silva AM, Young CC, Levitus S (1994) Atlas of surface marine data 1994. Anomalies of miscellaneous derived quantities, vol 5. NOAA Atlas NESDIS 10. US Department of Commerce, NOAA, NESDIS

Speer K, Tziperman E (1992) Rates of water mass formation in the North Atlantic Ocean. J Phys Oceanogr 22:93–104

Stommel H (1961) Thermohaline convection with two stable regimes of flow. Tellus 13:224–230

Stouffer RJ et al. (2006) Investigating the causes of the response of the thermohaline circulation to past and future climate changes. J Clim 19:1365–1387

Stouffer RJ, Manabe S (2003) Equilibrium response of thermohaline circulation to large changes in atmospheric CO_2 concentration. Clim Dyn 20:759–773

Tziperman E (1986) On the role of interior mixing and air–sea fluxes in determining the stratification and circulation of the ocean. J Phys Oceanogr 16:680–693

Tziperman E (2000) Uncertainties in thermohaline circulation response to greenhouse warming. Geophys Res Let 27:3077–3080

Uppala SM et al (2005) The ERA-40 re-analysis. Q J R Meteorol Soc 131:2961–3012

Valcke S, Declat D, Redler R, Ritzdorf H, Schoenemeyer T, Vogelsang R (1004) Proceedings of the 6th international meeting. High performance computing for computational science, vol 1. Universidad Politecnica de Valencia, Valencia, Spain. The PRISM coupling and I/O system. VEC-PAR'04

Vellinga M, Wood RA, Gregory JM (2002) Processes governing the recovery of a perturbed thermohaline circulation in HadCM3. J Clim 15:764–780

Walin G (1982) On the relation between sea-surface heat flow and thermal circulation in the ocean. Tellus 34:187–195

Wijffels SE, Schmitt RW, Bryden HL, Stigebrandt A (1992) Transport of freshwater by the oceans. J Phys Oceanogr 22:155–162

Williams P, Guilyardi E, Sutton R, Gregory J, Madec G (2006) Tropical Pacific ocean adjustment to changes in the hydrological cycle in a coupled ocean–atmosphere model. Clim Dyn (in press)

Wood RA, Keen AB, Mitchell JFB, Gregory JM (1999) Changing spatial structure of the thermohaline circulation in response to atmospheric CO_2 forcing in a climate model. Nature 399:572–575